1-s2.0-S0022286015002811-main

DATASET · MAY 2015

READS
24

3 AUTHORS:

Gopi Ragupathy
Indira Gandhi Centre for Atomic Research
10 PUBLICATIONS **5** CITATIONS
SEE PROFILE

N. Ramanathan
Indira Gandhi Centre for Atomic Research
30 PUBLICATIONS **77** CITATIONS
SEE PROFILE

Kalyansundaram Sundararajan
Indira Gandhi Centre for Atomic Research
50 PUBLICATIONS **422** CITATIONS
SEE PROFILE

Journal of Molecular Structure 1094 (2015) 118–129

Contents lists available at ScienceDirect

Journal of Molecular Structure

journal homepage: www.elsevier.com/locate/molstruc

Acetonitrile–water hydrogen-bonded interaction: Matrix-isolation infrared and *ab initio* computation

R. Gopi, N. Ramanathan, K. Sundararajan *

Chemistry Group, Indira Gandhi Centre for Atomic Research, Kalpakkam 603 102, India

HIGHLIGHTS

- Experimental evidence for the formation of linear 1:1 CH_3CN—H_2O.
- Computation showed two minima a linear and cyclic complex.
- Computations were also carried out for 1:2 and 2:1 complexes of CH_3CN and H_2O.
- AIM and NBO analyses were carried out for the complexes A and B.

ARTICLE INFO

Article history:
Received 28 January 2015
Received in revised form 2 March 2015
Accepted 24 March 2015
Available online 8 April 2015

Keywords:
Ab initio computation
Hydrogen-bonded
Matrix-isolation
Acetonitrile
Water

ABSTRACT

The 1:1 hydrogen-bonded complex of acetonitrile (CH_3CN) and water (H_2O) was trapped in Ar and N_2 matrices and studied using infrared technique. *Ab initio* computations showed two types of complexes formed between CH_3CN and H_2O, a linear complex A with a C≡N···H interaction between nitrogen of CH_3CN and hydrogen of H_2O and a cyclic complex B, in which the interactions are between the hydrogen of CH_3CN with oxygen of H_2O and hydrogen of H_2O with π cloud of —C≡N of CH_3CN. Vibrational wavenumber calculations revealed that both the complexes A and B were minima on the potential energy surface. Interaction energies computed at B3LYP/6-311++G(d,p) showed that linear complex A is more stable than cyclic complex B. Computations identified a blue shift of ~11.5 cm^{-1} and a red shift of ~6.5 cm^{-1} in the CN stretching mode for the complexes A and B, respectively. Experimentally, we observed a blue shift of ~15.0 and ~8.3 cm^{-1} in N_2 and Ar matrices, respectively, in the CN stretching mode of CH_3CN, which supports the formation of complex A. The Onsager Self Consistent Reaction Field (SCRF) model was used to explain the influence of matrices on the complexes A and B. To understand the nature of the interactions, Atoms in Molecules (AIM) and Natural Bond Orbital (NBO) analyses were carried out for the complexes A and B.

Introduction

Acetonitrile (CH_3CN) is a simple organic nitrile detected in the gas phase in interstellar clouds [1]. CH_3CN has a unique property such as high relative permittivity (ε_r = 37.5) and hence possess remarkable miscibility with range of ionic and polar solvents [2], which makes CH_3CN as a solvent of choice for variety of organic synthesis. CH_3CN is also used as a mobile phase in HPLC and LC–MS. CH_3CN has been extensively used in synthetic organic chemistry.

Freedman and Nixon investigated the infrared spectra of CH_3CN in solid argon matrix [3]. Later, Kim and Kim re-investigated the vibrational spectra of CH_3CN using Fourier transform infrared spectra and made precise assignments of monomers, dimers and higher mulitmers of CH_3CN [4]. Givan and Loewenschuss studied the Raman spectrum of CH_3CN using matrix isolation spectroscopy [5]. Several groups have studied the H-bonded interaction of CH_3CN with a variety of electron acceptors [6–20].

Recently, we have reported the hydrogen-bonded interaction of CH_3CN with C_2H_2 in an Ar and N_2 matrices and found evidences for the formation of 1:1, 1:2 and 2:1 C_2H_2—CH_3CN complexes [21].

Interaction of CH_3CN with H_2O was studied extensively by many theoretical groups. Doo-sik Ahm and Sungyul Lee computationally studied the σ- and π-type hydrogen-bonded complexes of acetonitrile–water clusters. They found at MP2/6-31+G(d,p) level of theory the π-type complex to be slightly lower in ZPE corrected energy by 0.11 kcal/mol, while the σ-type complex is lower in energy by 0.09 kcal/mol at MP2/aug-cc-pVDZ level of theory [22]. Ajay chaudhari and Shyi-Long Lee using DFT/6-31+G(d) level of

* Corresponding author. Tel.: +91 44 27480098; fax: +91 44 27480065.
E-mail address: sundar@igcar.gov.in (K. Sundararajan).

http://dx.doi.org/10.1016/j.molstruc.2015.03.046
0022-2860/

theory studied the interaction of CH_3CN with one, two, and three water molecules. For the 1:1 $CH_3CN—H_2O$ complex, it was found that the cyclic structure is less stable than open structure [23].

Canuto et al. performed *ab initio* computations on the $CH_3CN\cdots H_2O$ complex to obtain the structure, vibrational frequencies, Rayleigh and Raman activities including light scattering depolarization and binding energies. All the theoretical models showed shortening of the CN distance, leading to a blue shift of around ~15 cm^{-1} in the CN stretching mode. In the Raman spectrum, the depolarization due to the intense CN stretching vibration was increased by 20% after the hydrogen bond formation. Further, there was a large red shift of 75 cm^{-1} in the OH mode of water, which leads to intensification of the Raman scattering activity [24].

Bako et al. [25] investigated the structure of $CH_3CN—H_2O$ mixture using *ab initio* computations, molecular dynamics and X-ray diffraction techniques. Computations showed two types of complexes; (a) H-bonded complex between the nitrogen of CH_3CN and hydrogen of H_2O and (b) CH_3CN and H_2O molecules are in side-by-side anti dipole arrangement. Both the complexes were minima on the potential energy surface, which have nearly the same interaction energy. They also confirmed the formation of microheterogeneity in the $CH_3CN—H_2O$ system.

Tabata et al. [26] studied the liquid structure of $CH_3CN—H_2O$ using X-ray diffraction and Infrared technique. They observed due to the dipole–dipole interaction between water and $CH_3CN—H_2O$, CH_3CN completely miscible with water at all concentration ratios. Furthermore, they found that $CH_3CN—H_2O$ and water clusters coexist, as microheterogeneity occurs in $CH_3CN—H_2O$ mixtures.

Chaban studied the interaction of three nitrile molecules, cynamide ($H_2N—C\equiv N$), CH_3CN and aminoacetonitrile ($H_2N—CH_2—C\equiv N$) with water molecules using second order Moller–Plesset perturbation theory with triple-ξ basis sets. For the $CH_3CN—H_2O$ system, *ab initio* computations identified two equilibrium geometries. The lowest energy complex was the one where the hydrogen of water molecule is bound to the C≡N end of the nitrile molecule through hydrogen bond and the second complex has two weak hydrogen bonds between CH_3CN and H_2O [27].

Allamandola et al. studied 16 nitriles and related compounds in Ar and H_2O matrices. The strong C≡N stretching vibrations of these compounds were probed using vibrational spectroscopy in matrices. They have compared the IR spectra in the C≡N stretching region of 19 nitriles in Ar and H_2O matrices. They observed two major bands for the CH_3CN molecule in the CN stretching region at 2258.3 cm^{-1} and 2293.0 cm^{-1} in Ar matrix. The low frequency band is assigned to the C≡N stretching vibration and the high frequency band is due to the combination band produced by the strong vibrational modes at 1376 and 917 cm^{-1}. In contrast, the CH_3CN spectrum in ice matrices is broad and the frequencies were

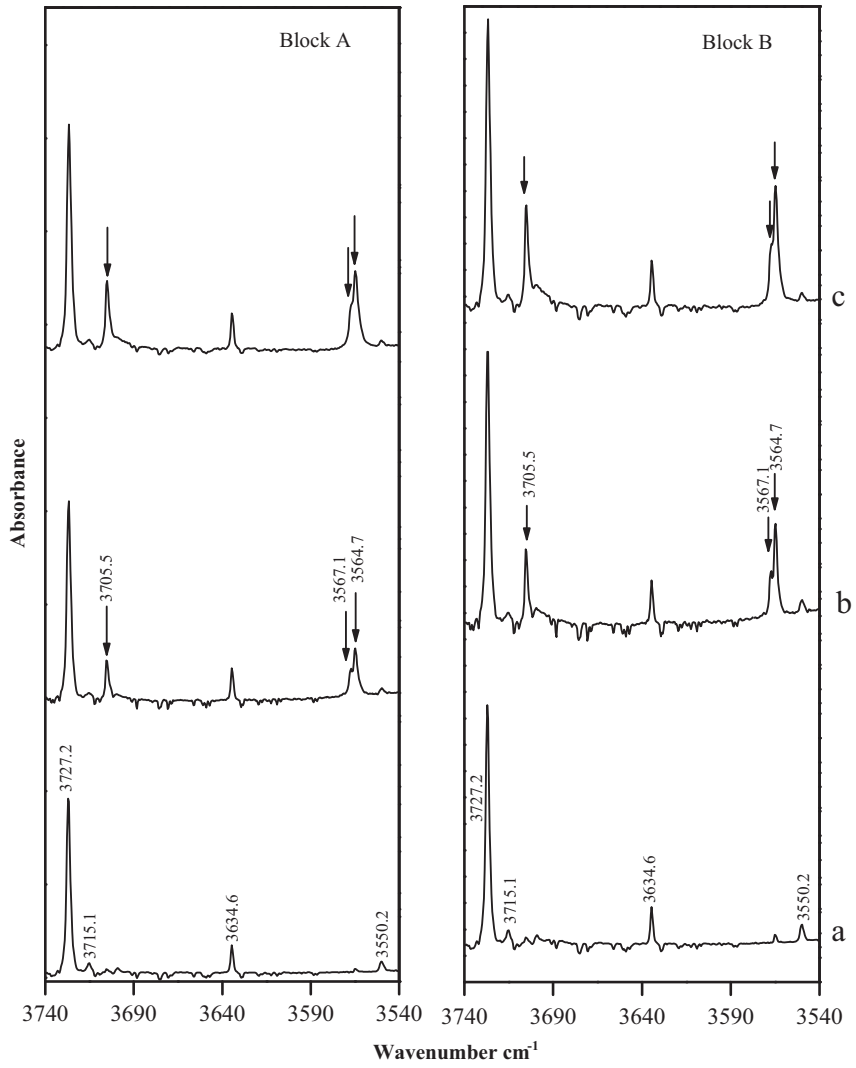

Fig. 1. Spectra of $CH_3CN—H_2O$ complexes in N_2 matrix in the region 3740–3540 cm^{-1}. Block A shows the as-deposited spectra and block B shows the 30 K annealed spectra. Matrix isolation infrared spectra of various concentrations of $CH_3CN/H_2O/N_2$; (a) 0/1/1000; (b)1/1/1000; (c) 2/1/1000.

shifted due to the strong intermolecular interactions. The absorption band of these nitriles in Ar and H_2O matrices are then used to facilitate the search for these features observed by Infrared Space Observatory (ISO) [28].

Eventhough, several theoretical groups have performed calculations on the $CH_3CN—H_2O$ system and found CH_3CN and H_2O form linear and cyclic type complexes, there is no clear experimental evidence for the formation of these complexes in the condensed phase. In this study, we have used matrix-isolation infrared technique and *ab initio* computations to identify the $CH_3CN—H_2O$ complex.

Experimental and computational methods

Matrix-isolation experiments were carried out using a Leybold closed cycle cryostat RDK-408D2 (Sumitomo Heavy Industries Ltd.). The entire cryostat unit along with the cold-tip was housed in a vacuum chamber and pumped through diffusion pump backed by rotary pump. The chamber was kept at a pressure of $<1 \times 10^{-6}$ mbar. The sample de-ionized and triple distilled H_2O and CH_3CN (Merck, HPLC grade 99.8%) were used as such, without further purification. Ar and N_2 (IOLAR Grade 2) was used as matrix gas. The H_2O, CH_3CN, N_2 or Ar gas was then deposited separately using triple jet nozzle onto a KBr substrate maintained at 12 K. We used typical matrix-to-sample ratios ranging from 1000:0.5 to 1000:1 for H_2O and 1000:0.5 to 1000:2.5 for CH_3CN. The matrix was then deposited at a typical rate of ~3 mmol/h and a deposition typically lasted for about 60 min.

Infrared spectra of the matrix isolated samples were recorded in the range 4000–400 cm^{-1}, using a BOMEM MB 100 FTIR spectrometer, operated at a resolution of 1 cm^{-1}. The matrix was then slowly warmed to 35 K for Ar and 30 K for N_2 which was maintained at this temperature for about 15 min and then re-cooled to 12 K. Spectra of the annealed matrices were again recorded.

Theoretical calculations were performed for the $CH_3CN—H_2O$ complexes using GAUSSIAN 94W suite of programs [29]. Geometries of the precursor molecules were first optimized at B3LYP/6-311++G(d,p) and MP2/aug-cc-pVDZ levels of theory. Starting from the optimized monomer geometries, the geometry of the 1:1 complexes was then optimized without imposing any constraints. Vibrational wavenumber calculations were performed for the optimized geometries to enable us to characterize the nature of the stationary points and also to assign the observed wavenumbers in our matrix isolation experiments. The computed wavenumbers were scaled on a mode by mode basis, where the scaling factors were arrived at as follows. The strongest feature in the spectrum of matrix isolated CH_3CN or H_2O that could be unambiguously assigned to these monomers, was correlated with

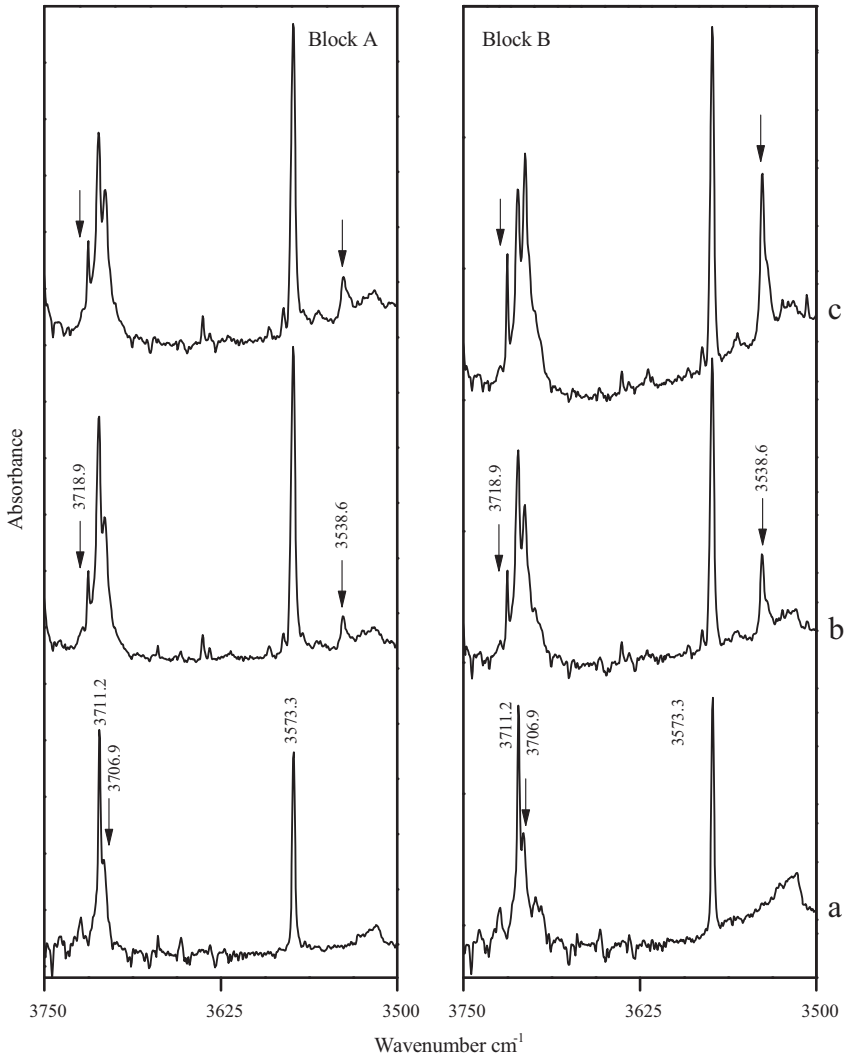

Fig. 2. Spectra of $CH_3CN—H_2O$ complexes in Ar matrix in the region 3750–3500 cm^{-1}. Block A and block B corresponds to the as-deposited and 35 K annealed spectra. Matrix isolation infrared spectra of various concentrations of $CH_3CN/H_2O/Ar$; (a) 0/0.5/1000; (b) 1.5/0.5/1000; (c) 2.5/0.5/1000.

the strongest computed feature for these species. The scaling factor that brought this computed frequency into agreement with the experimentally observed frequency was calculated; this scaling factor was used to scale all other vibrational wavenumbers of the hydrogen-bonded complex, in a given frequency region. For example, the ν_3 mode of *monomeric* H_2O was experimentally observed at 3727.2 cm^{-1} in N_2 matrix while the computed (unscaled) value for the same mode occurred at 3918.8 cm^{-1}; a scaling factor of 0.9511 is therefore indicated to bring the computed value for the monomer in agreement with the experimental value. This scaling factor was then used to scale the computed frequencies of the ν_3 mode of H_2O in the complex. It is recognized that the matrix perturbs the vibrational frequencies of the trapped species, with the magnitude of perturbation depending on the vibrational frequency of the mode. We therefore consider that a mode-by-mode scaling is an appropriate method to account for the varying degrees of matrix influence and helps in bringing the computations in better agreement with experimental values, over the entire range of the vibrational wavenumbers.

Interaction energies were computed for the complexes, corrected separately, for basis set superposition errors (BSSE) using the method outlined by Boys and Bernardi [30] and zero point energies.

Atoms-in-molecules (AIM) theory was applied to study the nature of the interaction in the $CH_3CN—H_2O$ complexes [31]. We searched for a (3, −1) bond critical point between the H_2O and CH_3CN sub-molecules, which could be associated with the intermolecular or intramolecular interaction using the AIM package [32]. The properties at this BCP, such as the electron density $\rho(r_c)$ and $\nabla^2\rho(r_c)$ were examined using the AIM package. It is well known that weak van der Waals type interactions are characterized by small values of $\rho(r_c)$ and $\nabla^2\rho(r_c) > 0$ [33]. In order to understand the nature of hyperconjugative charge-transfer interactions in the $CH_3CN—H_2O$ complexes, NBO (version 3.1) analysis was performed, invoked through Gaussian [34].

To understand the effect of the matrices on to the equilibrium geometries and energies of the $CH_3CN—H_2O$ complexes, calculations were performed using the Onsager self-consistent reaction field (SCRF) model, as implemented in the Gaussian program [35,36]. In this model, the solute molecule is placed in a spherical cavity surrounded by a continuum with constant dielectric properties. The molecular dipole induces a dipole in the dielectric medium and the electric field applied to the solute by the solvent dipole in turn interacts with the molecular dipole, altering the energy of the solute. The radius of the spherical cavity occupied by the solute was estimated based on molecular volumes obtained from the Gaussian calculations.

Results and discussion

Experimental details

Figs. 1 and 2 show the as-deposited (block A) and annealed spectra (block B) of H_2O with and without CH_3CN in N_2 and Ar matrices. In N_2 matrix, the ν_3 and ν_1 modes of H_2O were observed

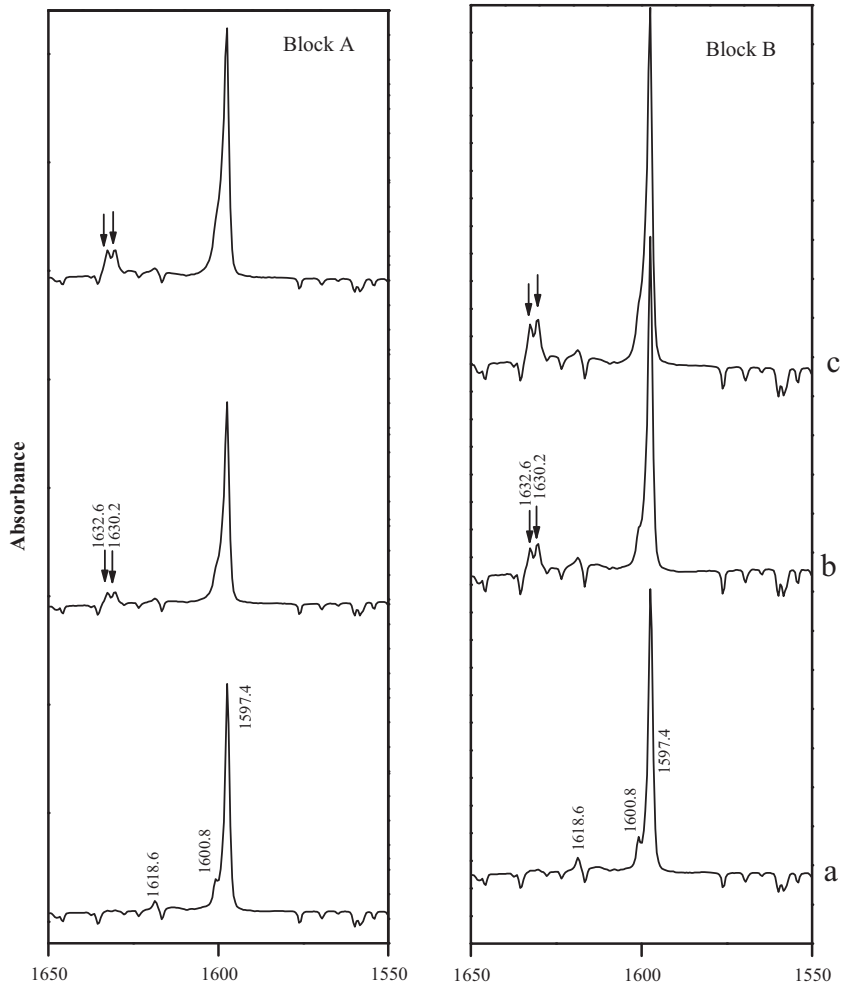

Fig. 3. Spectra of $CH_3CN—H_2O$ complexes in N_2 matrix in the region 1650–1550 cm^{-1}. Block A shows the as-deposited spectra and block B shows the 30 K annealed spectra. Matrix isolation infrared spectra of various concentrations of $CH_3CN/H_2O/N_2$; (a) 0/1/1000; (b) 1/1/1000; (c) 2/1/1000.

at 3727.2 cm^{-1} and 3634.6 cm^{-1} respectively. The feature observed at 3715.1 and 3550.2 cm^{-1} correspond to the ν_3 acceptor and ν_1 donor mode of $(H_2O)_2$ in N_2 matrix. In Ar matrix, the ν_3 mode of H_2O was observed at 3711.2 cm^{-1}. The feature observed at 3706.9 and 3573.3 cm^{-1} are due to ν_3 donor and ν_1 acceptor of $(H_2O)_2$ in Ar matrix, respectively. These features agree well with the reported literature value [37]. When H_2O and CH_3CN were co-deposited in N_2 and Ar matrix, new feature were observed in the ν_3 and ν_1 mode of H_2O in N_2 and Ar matrix at 3705.5, 3567.1/3564.7 cm^{-1} and 3718.9, 3538.6 cm^{-1}, respectively. Furthermore, the intensity of these features increased on annealing the matrix.

Fig. 3 shows the IR spectra of the ν_2 mode of H_2O in N_2 matrix. Block A and B correspond to the spectra recorded at 12 K and after annealing at 30 K. The feature observed at 1597.4 cm^{-1} is due to ν_2 mode of water in N_2 matrix. The features observed at 1618.6 and 1600.8 cm^{-1} are due to ν_2 donor and acceptor mode of $(H_2O)_2$ in N_2 matrix. Co-deposition of H_2O and CH_3CN and subsequent annealing produced a doublet at 1630.2/1632.6 cm^{-1}. In Ar matrix, the ν_2 bending mode of H_2O is complex due to the vibration–rotation structure and new features could not be discerned in this region and hence not shown.

Figs. 4 and 5 show the IR spectra of CN stretching mode of CH_3CN in N_2 and Ar matrix. Figs. 4 and 5a show the spectra of CH_3CN in N_2 and Ar matrices. The features observed at 2257.5 and 2257.9 cm^{-1} are due to ν_2 CN stretch mode of CH_3CN in N_2 and Ar matrix, whereas the feature observed at 2266.2 cm^{-1} in N_2 matrix is also due to CH_3CN monomer trapped in a different site [38]. Features due to acetonitrile dimer $(CH_3CN)_2$ in N_2 and Ar matrices were observed at 2254.6 and 2256.0 cm^{-1}, respectively. When H_2O and CH_3CN were co-deposited, new feature was observed at 2272.5 cm^{-1} in N_2 and a doublet at 2264.7/2267.6 cm^{-1} in Ar matrix.

Experiments were performed where CH_3CN and H_2O alone were deposited separately in the N_2 and Ar matrices to confirm that all the product features discussed in this work did correspond to the adducts of CH_3CN with H_2O. Unfortunately, in experiments where CH_3CN alone was deposited, H_2O was found to be present as an inevitable impurity (Figs. 4 and 5a). However, the dependence of the intensity of the product features on the H_2O concentration confirmed the participation of both CH_3CN and H_2O in the complex formation. New features could not be observed in the ν_4 CC stretch, ν_7 CH_3 rocking, ν_3 CH_3 deformation, ν_6 antisymmetric CH_3 deformation, ν_1 symmetric CH stretching, ν_5 antisymmetric CH stretching modes of CH_3CN in both Ar and N_2 matrices as these vibrational modes resulted in a smaller infrared absorption intensity on complex formation.

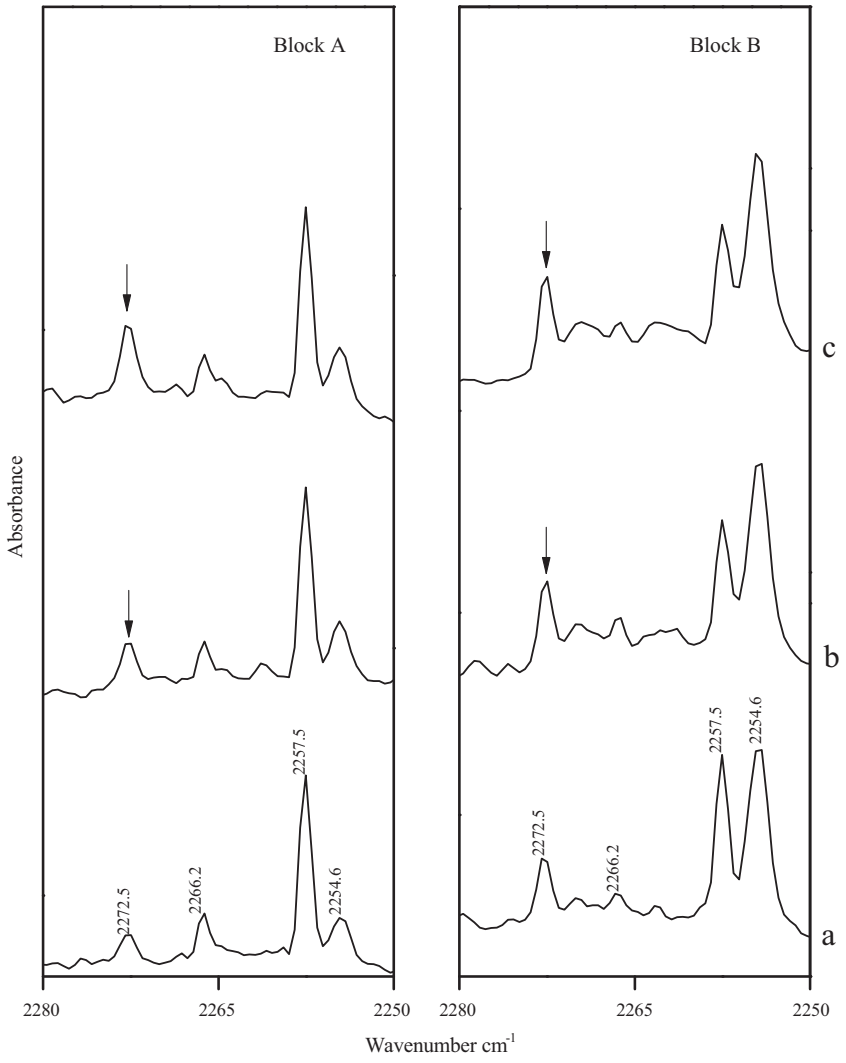

Fig. 4. Spectra of CH_3CN—H_2O complexes in N_2 matrix in the region 2280–2250 cm^{-1}. Matrix isolation infrared spectra of various concentrations of $CH_3CN/H_2O/N_2$; (a) 2.5/0/1000; (b) 2.5/0.5/1000; (c) 2.5/0.75/1000. Block A shows the as-deposited spectra and block shows the 30 K annealed spectra.

Computations on the $CH_3CN—H_2O$ complexes

Several groups [22–27] have performed extensive calculations on the $CH_3CN—H_2O$ system. All the computations invariably showed that CH_3CN and H_2O form two types of complexes; (a) a linear complex, global minimum, where the nitrogen of CH_3CN interacts with the hydrogen of H_2O and (b) a cyclic complex, local minimum, where the hydrogen of CH_3CN interacts with oxygen of H_2O and hydrogen of H_2O interacts with the π cloud of —C≡N of CH_3CN. Depending upon the level of theory and basis set used in the computations the interaction energies of these complexes varied. Our computations also identified two minima on the potential energy surface, where the global minimum was the linear complex, A, and the cyclic complex B was the local minimum. Fig. 6 shows the structure of these complexes computed at B3LYP/6-311++G(d,p) level of theory. Table 1 shows the selected structural parameters for the complexes A and B computed at this level. For the complex A, the bond distance between 6N···7H is 2.0805 Å. Due to this hydrogen-bonded interaction, the O—H bond is elongated by 0.006 Å and the C≡N bond distance is decreased by 0.001 Å. For the complex B, the bond distance between the 2H···7O is 2.6883 Å and there is another interaction between 9H···6N and 9H···5C, the bond distances are 2.4755 Å and 2.5095 Å, respectively. The O—H and C≡N bond distance in the complex B are elongated by 0.001 Å and 0.006 Å, respectively. Table 2 shows the calculated interaction energies for the complexes A and B computed at B3LYP/6-311++G(d,p) level of theory. As can be seen from the table, the raw interaction energies of the two complexes are −4.82 and −3.91 kcal/mol, which reduces to −3.43 and −2.67 kcal/mol when zero-point energy corrections are applied. Further, the relative energy difference between the raw energies for the two complexes A and B at B3LYP/6-311++G(d,p) and MP2/aug-cc-pVDZ are −0.91 and −0.12 kcal/mol respectively. It can be seen from the table that at all levels of theory and basis sets used, complex A is more stable than complex B.

Vibrational assignments

The experimental vibrational wavenumbers of the $CH_3CN—H_2O$ complexes A and B were compared with the wavenumber calculated using B3LYP/6-311++G(d,p) level of theory. (Table 3).

Table 4 compares the shift between the scaled computed vibrational wavenumbers with experimental wavenumbers in N_2 and Ar matrices for the complex A.

ν_3 and ν_1 modes of H_2O

DFT computations indicated due to the hydrogen bonding in complex A, the ν_3 and ν_1 mode of H_2O are red shifted by 25.5

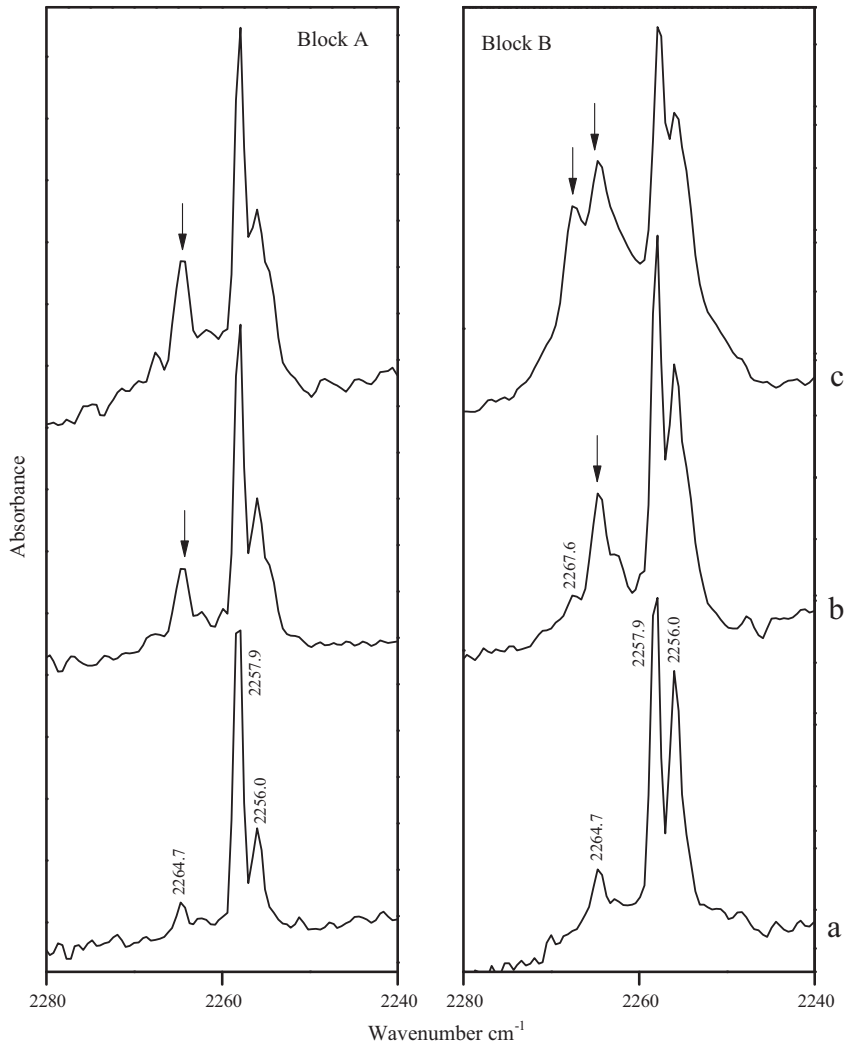

Fig. 5. Spectra of $CH_3CN—H_2O$ complexes in Ar matrix in the region 2280–2240 cm^{-1}. Matrix isolation infrared spectra of various concentrations of $CH_3CN/H_2O/N_2$; (a) 1.5/0/1000; (b) 1.5/0.5/1000; (c) 1.5/0.75/1000. Block A shows the as-deposited spectra and block B shows the 35 K annealed spectra.

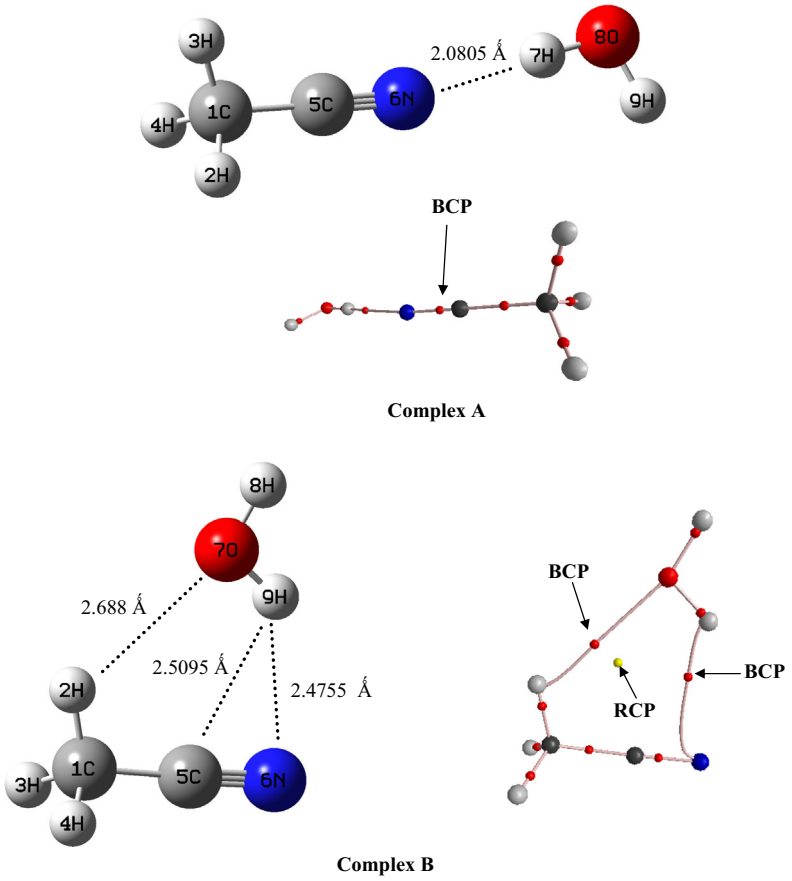

Fig. 6. Structure of the $CH_3CN—H_2O$ complexes A and B optimized at B3LYP/6-311++G(d,p) level of theory.

Table 1
Selected parameters[a] for the $CH_3CN—H_2O$ complex A Calculated at B3LYP/6-311++G(d,p) level of theory.

Parameter	Complex A	Parameter	Complex B
C1—H2	1.0917 (1.0919)[b]	C1—H2	1.0921 (1.0919)
C1—H3	1.0917 (1.0919)	C1—H3	1.0917 (1.0919)
C1—H4	1.0917 (1.0919)	C1—H4	1.0917 (1.0919)
C1—C5	1.4550 (1.4570)	C1—C5	1.4549 (1.4570)
C5—N6	1.1513 (1.1527)	C5—N6	1.1533 (1.1527)
N6—H7	2.0805	H2—O7	2.6883
C5—H9	4.5584	C5—H9	2.5095
N6—H9	3.4095	N6—H9	2.4755
H7—O8	0.9685 (0.9625)	O7—H8	0.9615 (0.9625)
O8—H9	0.9612 (0.9622)	O7—H9	0.9651 (0.9622)
∠H2—C1—H3	108.9 (108.8)	∠H2—C1—H3	109.3 (108.8)
∠H2—C1—C5	110.1 (110.1)	∠H2—C1—C5	108.7 (109.5)
∠C1—C5—N6	179.9 (179.9)	∠C1—C5—N6	178.0 (180.0)
∠C5—N6—H7	168.1	∠C1—H2—O7	120.1
∠N6—H7—O8	178.8	∠C5—N6—H9	82.5
∠H7—O8—H9	104.7 (105.1)	tor∠C5—N6—H9—O7	0.0
tor∠N6—H7—O8—H9	5.5	tor∠H4—C1—H2—O7	120.5
tor∠C1—C5—N6—H7	8.5	tor∠O7—H2—C1—C5	0.08

[a] Bond length in Å; bond angle and dihedral angle in °.
[b] Numbers in parenthesis are those of uncomplexed molecule.

and 74.9 cm^{-1} respectively. Experimentally, we observed new features at 3705.5 and 3564.7/3567.1 cm^{-1} in N_2 and at 3718.9 and 3538.6 cm^{-1} in Ar matrices, which amounts to a red shift of 21.7,68.7 cm^{-1} and 14.1, 99.4 cm^{-1}, respectively. The experimental shift compares well with the scaled computed wavenumbers for the complex A.

The features observed at 3564.7/3567.1 cm^{-1} in the ν_1 mode of H_2O may be due to the matrix splitting in N_2 matrix for the complex A.

It should be mentioned that for the complex A, computation shows the IR intensity of the ν_1 symmetric stretching mode of H_2O increases by a factor of ~40 whereas the same mode in the complex B increases only by a factor of ~3 when compared to the H_2O monomer.

ν_2 mode of H_2O

In N_2 matrix, the ν_2 mode for the complex A is observed as a site split feature at 1630.2 and 1632.6 cm^{-1}, a blue shift of 34.0 cm^{-1}

Table 2
Raw[a]/ZPE-Corrected/BSSE-corrected interaction energies for the $CH_3CN—H_2O$ complexes A and B computed at B3LYP/6-311++G(d,p) and MP2/aug-cc-pVDZ levels of theory.

Interaction energy (ΔE) (kcal/mol)		
Complex	B3LYP/6-311++G(d,p)	MP2/aug-cc-pVDZ
A	−4.82/−3.43/−4.50	−5.32/−3.91/−4.45
B	−3.91/−2.67/−3.79	−5.20/−3.81/−4.36

[a] Raw interaction energies refer to energies not corrected for either ZPE or BSSE.

from the monomeric H_2O feature. The computations also showed a similar trend, i.e., the computed value for the complex A occurs at 1632.1 cm^{-1}, a blue shift of 28.9 cm^{-1}, which compares well with the experimentally observed feature at 1630.2 cm^{-1}. The complexity in the ν_2 mode of H_2O in Ar matrix due to vibration–rotation congestion did not enable us to clearly discern the new feature for the complex.

ν_2 CN stretch of CH_3CN

The computed value in this mode for the complex A occurs at 2373.7 cm^{-1}, a blue shift of 11.5 cm^{-1}. In N_2 matrix, on complex formation new feature was observed at 2272.5 cm^{-1}, and in Ar matrix as a doublet at 2264.7/2267.6 cm^{-1}, a blue shift 15.0 and 8.3 cm^{-1}, respectively, which agrees well with the computed feature for the complex A. It should be mentioned that computed value for the complex B shows a red shift of 7.2 cm^{-1}. Experimentally, we could observe only the blue-shifted feature with respect to the CH_3CN monomer, which clearly ascertains the formation of complex A in both the matrices.

Onsager solvation model

In order to understand the effects of the N_2 and Ar matrices on to the structure and energetics of the $CH_3CN—H_2O$ complexes A and B, the structures of the two complexes were optimized within the Onsager reaction field model. The value of the dielectric constant ε was set equal to 2.00 and 1.43, which were appropriate for the N_2 and Ar matrices, respectively [39–41]. We performed SCRF single point energy calculation at the B3LYP/6-311++G(d,p) level of theory for the $CH_3CN—H_2O$ complexes A and B. Table 5 gives the relative raw energies of the complexes A and B in the N_2 and Ar matrices computed at B3LYP/6-311++G(d,p) level of theory. As can be seen from the table that the complex A is stabilized

Table 4
Shift in the scaled computed and experimental vibrational wavenumbers for the $CH_3CN—H_2O$ complex A computed at B3LYP/6-311++G(d,p) level of theory.

Mode	$\Delta\nu^a_{cal}$ (cm^{-1})	$\Delta\nu^a_{exp}$ (cm^{-1})	$\Delta\nu^a_{cal}$ (cm^{-1})	$\Delta\nu^a_{exp}$ (cm^{-1})
	Ar		N_2	
ν_2 CN stretching	+10.3	+8.3	+11.1	+15.0
ν_1 mode of H_2O	−71.4	−99.4	−71.3	−68.7
ν_2 mode of H_2O	+28.6	–[b]	+28.8	+34.0
ν_3 mode of H_2O	−24.3	−14.1	−24.3	−21.7

[a] $(\Delta\nu)_{expt/calc} = (\nu_{complex} - \nu_{monomer})$.
[b] Experimental features not observed.

Table 5
Influence of dielectric constant on the raw energies of the $CH_3CN—H_2O$ complexes A and B calculated at B3LYP/6-311++G(d,p) level of theory, using the Onsager solvation model.

Complex	Dipole moment (D)[a]	Interaction energy (ΔE) (kcal/mol)		
		Gas (0.00)[b]	Nitrogen (2.00)[b]	Argon (1.43)[b]
Complex A	6.20	−4.82	−5.63	−5.24
Complex B	2.26	−3.91	−2.16	−2.95

[a] Dipole moment in Debye.
[b] Dielectric constant of the medium.

Table 3
Computed unscaled and scaled vibrational wavenumbers, scaling factors and mode assignments calculated at the B3LYP/6-311++G(d,p) level and comparison with the experimental wavenumbers for the $CH_3CN—H_2O$ Complexes A and B in Ar and N_2 matrices.

Computed/unscaled ν (cm^{-1})	Ar			N_2			Mode assignment
	Computed/scaled ν (cm^{-1})	Scaling factor	Exp ν (cm^{-1})	Computed/scaled ν (cm^{-1})	Scaling factor	Exp ν (cm^{-1})	
Acetonitrile							
930.0(2)[a]	917.2	0.9856	916.6	917.6	0.9967	917.6	ν_4 sym. CC str. (A_1)
1061.0(2)	1038.2	0.9785	1038.2	1043.3	0.9833	1040.7/1045.8	ν_7 CH_3 rock (E)
1411.6(3)	1375.9	0.9747	1375.9	1378.5	0.9766	1378.5	ν_3 sym.CH_3 def (A_1)
1474.7(12)	1445.5	0.9802	1445.5	1447.9	0.9818	1446.7/1449.1	ν_6 antisym.CH_3 def. (E)
2362.9(12)	2258.0	0.9556	2258.0	2257.5	0.9557	2257.5	ν_2 CN str. (A_1)
3045.9(4)	2950.6	0.9687	2950.5	2949.0	0.9682	2949.0	ν_1 CH str. (A_1)
3115.6(1)	3004.4	0.9643	3004.5	3009.3	0.9659	3009.3	ν_5 antisym. CH str. (E)
H_2O							
3813.5(9)	3638.0	0.9540	3638.0	3634.6	0.9531	3634.6	ν_1 mode of H_2O
1603.2(66)[a]	1589.7	0.9916	1589.7/1608.0 1623.9	1597.4	0.9964	1597.4	ν_2 mode of H_2O
3918.8(57)	3733.0	0.9526	3776.4/3756.2/3711.2	3727.2	0.9511	3727.2	ν_3 mode of H_2O
Complex A							
2373.7(24)	2268.3	0.9556	2264.7/2267.6	2268.6	0.9557	2272.5	ν_2 C—N mode of CH_3CN
3738.6(368)	3566.6	0.9540	3538.6	3563.3	0.9531	3564.7/3567.1	ν_1 mode of H_2O
1632.1(60)	1618.3	0.9916	–[b]	1626.2	0.9964	1630.2/1632.6	ν_2 mode of H_2O
3893.3(111)	3708.7	0.9526	3718.9	3702.9	0.9511	3705.5	ν_3 mode of H_2O
Complex B							
2355.7(20)	2251.1	0.9556	–[b]	2251.3	0.9557	–[b]	ν_2 C—N mode of CH_3CN
3789.4(32)	3615.1	0.9540	–[b]	3611.7	0.9531	–[b]	ν_1 mode of H_2O
1611.4(97)	1597.9	0.9916	–[b]	1605.6	0.9964	–[b]	ν_2 mode of H_2O
3906.9(90)	3721.4	0.9526	–[b]	3715.9	0.9511	–[b]	ν_3 mode of H_2O

[a] Infrared intensities in kcal/mol are given ion parenthesis.
[b] Experimental feature not observed.

Table 6
Properties of (3, −1) bond critical points in the $CH_3CN—H_2O$ complexes A and B computed at the B3LYP/6-311++G(d,p) level.

Molecule		$\rho(r_c)$	$\nabla^2\rho(r_c)$	λ_1	λ_2	λ_3
(A) Intermolecular bond critical points in $CH_3CN—H_2O$ complexes						
Complex A	C≡N(AN)...H—O(H_2O)	0.0187	0.0689	−0.0230	−0.0223	0.1142
Complex B	C—H(AN)...O—H(H_2O)	0.0059	0.0217	−0.0047	−0.0038	0.0302
	O—H(H_2O)... C≡N(AN)	0.0094	0.0339	−0.0079	−0.0043	0.0462
(B) Bond critical point corresponding to the C≡N bond in CH_3CN, and $CH_3CN—H_2O$ complexes						
CH_3CN		0.4802	−0.2628	−1.0285	−1.0285	1.7940
Complex A		0.4799	−0.2517	−1.0356	−1.0340	1.8179
Complex B		0.4802	−0.2980	−1.0403	−1.0330	1.7753
(C) Bond critical point corresponding to the O—H in H_2O and $CH_3CN—H_2O$ complexes						
H_2O		0.3664	−2.4926	−1.7763	−1.7321	1.0158
Complex A		0.3572	−2.4938	−1.7806	−1.7405	1.0272
Complex B		0.3617	−2.5038	−1.7836	−1.7415	1.0214

Table 7
Electron occupancies of various NBOs of $CH_3CN—H_2O$ complexes A, and B computed at B3LYP/6-311++G(d,p) basis set. The donor–acceptor delocalization interaction and delocalization energies (E_2, kcal/mol) are also shown.

Complex	NBO	Occupancy	Donor–acceptor delocalization interaction	Second order perturbation (E_2) energy (kcal/mol)
A	n^1N6	1.96302 (1.96983)[a]	n^1N6 → σ*(H7—O8)	4.37
	σ*(H7—O8)	0.00971 (0.00002)[b]	σ(H7—O8) → σ*(C5—N6)	0.17
	σ*(C5—N6)	0.01182(0.01089)[a]	n^1O8 → σ*(C5—N6)	0.11
B	π(2)(C5—N6)	1.98691(1.98712)[a]	π(2)(C5—N6) → σ*(O7—H9)	0.52
	σ*(O7—H9)	(0.00217)(0.00002)[b]	π(2)(C5—N6) → σ*(O7—H8)	0.09
	σ*(O7—H8)	(0.00043)(0.00002)[b]		
	n^2 O7	1.99612(1.99689)[b]	n^2 O7 → σ*(1)(C1—H2)	0.27
			n^2 O7 → σ*(2)(C1—H2)	0.27
			σ(O7—H9) → π*(2)(C5—N6)	0.05

[a] Occupancy of monomeric CH_3CN is given in parenthesis.
[b] Occupancy of monomeric H_2 O is given in parenthesis.

by −0.81 (N_2) and −0.42 (Ar) kcal/mol, whereas the complex B is destabilized by 1.75 (N_2) and 1.00 (Ar) kcal/mol. It should be mentioned that the dipole moments of the complexes A and B were found to be 6.20 D and 2.26 D at B3LYP/6-311++G(d,p) level of theory, respectively. To summarize, the Onsager model indicates that the complex A is stabilized more than the complex B, due to the higher dipole moment of the former, when the solvent effects of the N_2 and Ar matrices were taken into account, which lends support to our assignments of the observed vibrational features in the two matrices *only* to complex A.

Nature of the interaction

AIM theory was used to analyze the nature of the interaction in the $CH_3CN—H_2O$ complexes. According to AIM analysis, H-bonding is the result of overlap of electron densities of the lone pair and hydrogen, which results in a charge transfer from donor to the acceptor atom. A (3, −1) bond critical point (BCP) was searched using the optimized geometry of the $CH_3CN—H_2O$ complexes A and B computed at B3LYP/6-311++G(d,p) level of theory. At the BCP for both the complexes A and B, electron density ($\rho(r_c)$), Laplacian of electron density ($\nabla^2\rho(r_c)$) were examined. Table 6a gives the properties of the intermolecular (3, −1) BCP for the complexes A and B. At the BCP for both the complexes A and B the values of ($\rho(r_c)$) were found to be of the order of 10^{-2} au, ($\nabla^2\rho(r_c)$) were positive, as are typical of closed shell interaction. Further, two (3, −1) BCP's were located for the complex B, one between the hydrogen of CH_3CN and oxygen of H_2O and another between hydrogen of H_2O and nitrogen of CH_3CN, confirming the cyclic nature of the complex. The comparison of the BCPs revealed that the magnitude of electron density $\rho(r_c)$ and Laplacian of electron density ($\nabla^2\rho(r_c)$) as a result of C—H···N interaction is higher in complex A than complex B.

BCPs corresponding to the C≡N bonds of CH_3CN and O—H bond of H_2O in the complexes were evaluated to understand the effect of intramolecular interaction on the neighboring bonds in the sub-molecules. Table 6b and c gives the properties for these BCPs. In the same table the values for the monomeric CH_3CN and H_2O are given for comparison. The high positive values of electron density and high negative values of the Laplacian clearly indicates a shared nature of interactions in the neighboring bonds of the sub-molecules of the $CH_3CN—H_2O$ complexes.

NBO analysis

NBO analysis was carried out to correlate the extent of red-shifting with the charge-transfer hyperconjugative interactions. The NBO analysis is a useful tool and provides insight on to the nature of the interactions particularly of red-shifted type [42–55]. The stabilizing interactions that arise due to the hyperconjugative interaction (n–σ*) in the H-bonded complexes is responsible for the origin of bond lengthening, which results in red-shift of vibrational wavenumber.

In NBO analysis, off-diagonal elements of the Fock matrix in the NBO basis give the measure of delocalization effects. The second-order perturbation energy (E_2) gives an estimate of the strength of these delocalization interactions.

The charge-transfer effect successfully explains the red-shifted H-bonding as a result of delocalization of the nitrogen lone pair. The results of NBO analysis of $CH_3CN—H_2O$ complexes A and B computed at B3LYP/6-311++G(d,p) level of theory are shown in Table 7. From the table it is clear that due to the hyperconjugative interaction between n^1N6 → σ*(H7—O8) for the complex A the electron occupancy of anti-bonding orbital σ*(H7—O8) of the H_2O sub-molecule increased by ∼0.00969e relative to the H_2O monomer. Similarly, a reduction in electron occupancies by ∼0.00679e was noticed for n^1N6 non-bonding orbital for the

CH_3CN sub-molecule in the complex A with respect to the CH_3CN monomer. The second order perturbation energy for this interaction is found to be ~4.37 kcal/mol. As can be seen from Table 7 in complex A apart from charge transfer interaction there is *bond pair-acceptor orbital interaction* $\sigma(H7—O8) \rightarrow \sigma^*(C5—N6)$ and $n^1O8 \rightarrow \sigma^*(C5—N6)$ due to which, the electron occupancy in the antibonding $\sigma^*(C5—N6)$ increases marginally by 0.0009e, and the corresponding E_2 energy of this interaction was found to be ~0.17 and ~0.11 kcal/mol, respectively.

Interestingly, for the complex B, the stabilization does not stem from the delocalization of nitrogen lone pair to anti bonding O7—H9 acceptor orbital as the nitrogen lone pair does not have the linear orientation (~180°) for the facile delocalization. This orientational effect likely precludes the interaction originating from lone pair on nitrogen. Nevertheless, complex B is stabilized due to the delocalization of C≡N π electrons to the acceptor orbital of H_2O moiety as it is evident from the marginal decrease in the occupancy of π (2) (C5—N6) orbital by 0.00021 e with the concomitant increase in the acceptor, $\sigma^*(O7—H9)$ orbital by 0.00215 e. The corresponding E_2 energy for this interaction was found to be ~0.52 kcal/mol. Being cyclic, complex B also gets extra stabilization due to the $n^2O7 \rightarrow \sigma^*(C1—H2)$ delocalization and the E_2 energy for such delocalization was ~0.27 kcal/mol.

Computations on the 1:2 and 2:1 $CH_3CN—H_2O$ complexes

To find out the possible sites of attack of the next H_2O or CH_3CN molecule on the $CH_3CN—H_2O$ complex *ab initio* computations were carried out for the higher complexes. Two minimum energy structure with $CH_3CN—(H_2O)_2$ (C and D) were obtained in the potential energy surface while one minima was found for $(CH_3CN)_2—H_2O$ (E). Fig. 7 shows the structure of these complexes. The higher complex C is stabilized by both C≡N···H and C—H···O interaction while the complex D is stabilized by O—H···π and C—H···O interactions. The

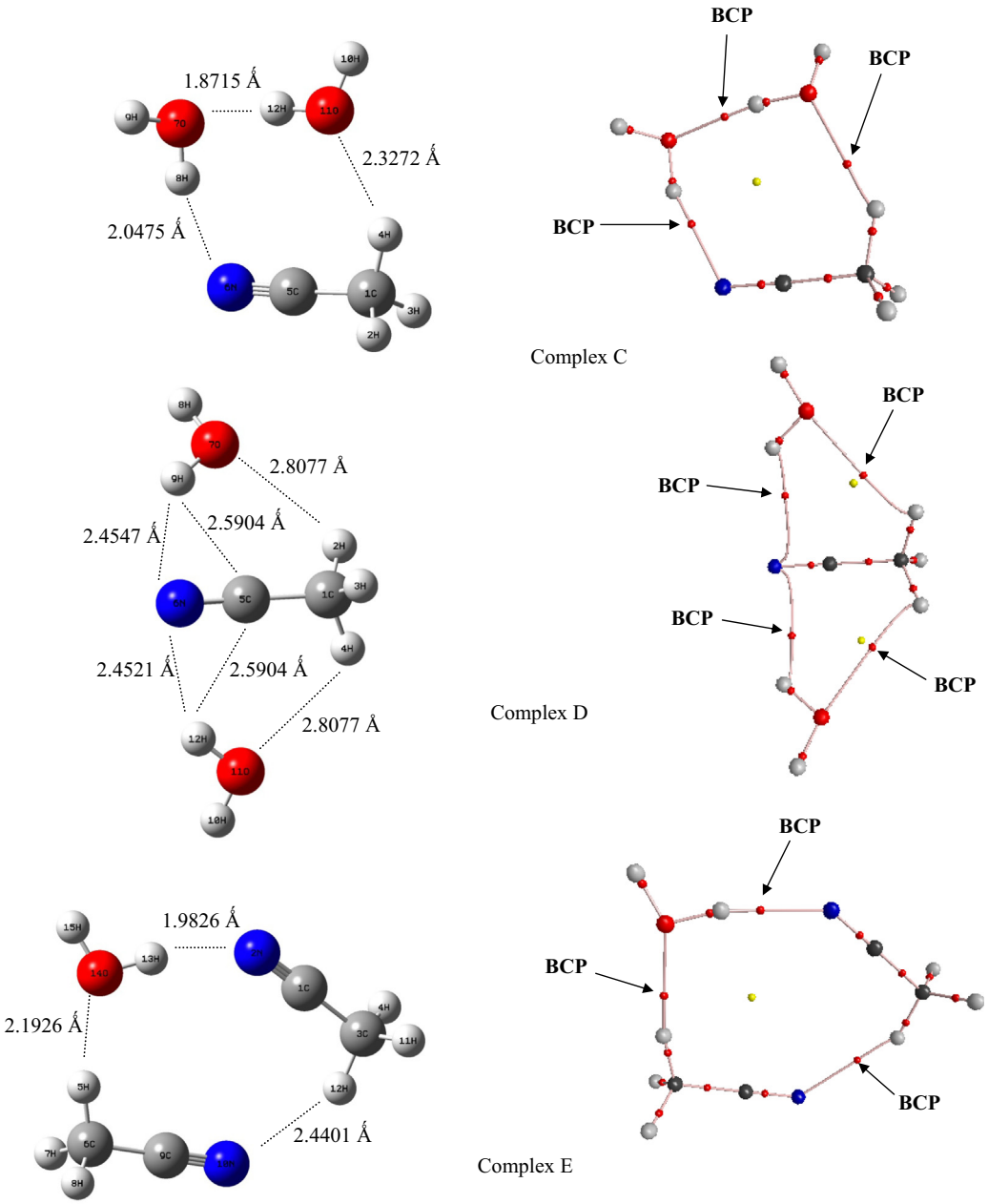

Fig. 7. Structure of the $CH_3CN—H_2O$ higher complexes C, D and E optimized at B3LYP/6-311++G(d,p) level of theory.

complex E is stabilized by O—H···N, C—H···N and C—H···O interactions.

Table 8 gives the stabilization energies for the higher complexes C, D and E computed at B3LYP/6-311++G(d,p) levels of theory. The ZPE-corrected energy for complex C is exothermic by 10.38 kcal/mol whereas for the complex D and E was found to be 5.10 and 9.53 kcal/mol, respectively. It should be mentioned that 1:2 and 2:1 higher complexes form cyclic structures. For the complex C and D, due to the interaction of CH_3CN with H_2O, the C≡N vibrational wavenumber are red-shifted by 7.6 cm^{-1} and 13.1 cm^{-1}, respectively, with respect to the CH_3CN monomer. For the complex E, the C≡N vibrational wavenumber are red-shifted and blue shifted by 9.3 cm^{-1} and 2.2 cm^{-1}, respectively. The structural parameters and the vibrational wavenumbers are given in supplementary information. It should be mentioned we could not discern any new features in our experiments due to higher complexes in both the matrices.

Relative shifts in the ν_2 CN mode of CH_3CN sub-molecule in $CH_3CN—C_2H_2$ and $CH_3CN—H_2O$ complexes

In our earlier work on the $CH_3CN—C_2H_2$ system [21], we obtained only one minimum for the 1:1 $CH_3CN—C_2H_2$ complex; in which hydrogen of acetylene interacts with the nitrogen of acetonitrile, where acetylene is the proton donor and nitrogen is the proton acceptor. Experimentally, the 1:1 $CH_3CN—C_2H_2$ complex was identified in both N_2 and Ar matrices. Table 9 shows the experimental shift, unscaled calculated shifts in the ν_2 CN stretch of CH_3CN and ZPE corrected stabilization energies for the $CH_3CN—C_2H_2$ and $CH_3CN—H_2O$ complexes.

The shift in the ν_2 CN mode of CH_3CN sub-molecule is a good indicator of the strength of the interaction in the complex. The experimental shift in the ν_2 CN stretch of CH_3CN sub-molecule in the $CH_3CN—C_2H_2$ and $CH_3CN—H_2O$ complexes are 5.9 and 8.3 cm^{-1}, respectively, where CH_3CN acts as a proton acceptor in these complexes. The ZPE corrected stabilization energy computed at B3LYP/6-311++G(d,p) level of theory for these complexes −2.0 and −3.4 kcal/mol, which is keeping in trend with the shifts in the vibrational frequency of the C—N stretch in CH_3CN. The above shift in the ν_2 CN mode of CH_3CN sub-molecule and the stabilization energy clearly indicates that H_2O forms a stronger complex than C_2H_2, which is consistent with the acidity of the H_2O and C_2H_2.

Table 8
Raw[a]/ZPE-corrected/BSSE-corrected interaction energies in kcal/mol for the $CH_3CN—H_2O$ higher complexes C, D and E Computed at B3LYP/6-311++G(d,p) levels of theory.

Complex	Interaction energy (ΔE) B3LYP/6-311++G(d, p)
C	−14.46/−10.38/−13.51
D	−7.40/−5.10/−7.11
E	−12.19/−9.53/−11.58

[a] Raw interaction energies refer to energies not corrected for either ZPE or BSSE.

Table 9
Comparison of experimental shift in Ar matrix with the scaled calculated shifts of ν_2 CN mode of CH_3CN and ZPE corrected energies in kcal/mol computed at B3LYP/6-311++G(d,p) level of theory for the 1:1 $CH_3CN—H_2O$ and $CH_3CN—C_2H_2$ complex.

Molecule	ν_{exp}	$\Delta\nu^a_{exp}$	ν_{cal}	$\Delta\nu^a_{cal}$	ΔE_{ZPE}
CH_3CN	2258.0	–	2258.0	–	–
$CH_3CN—H_2O$	2264.7/2267.6	8.3	2268.3	10.3	−3.4
$CH_3CN—C_2H_2$	2265.7/2263.8	6.8	2263.6	5.6	−2.0

[a] $(\Delta\nu)_{expt/calc} = (\nu_{monomer} - \nu_{complex})$.

Conclusion

Using matrix-isolation infrared spectroscopy, we have experimentally found evidences for the 1:1 $CH_3CN—H_2O$ complex A, which is stabilized by C≡N···H interaction. Computations performed at B3LYP/6-311++G(d,p) level of theory on the $CH_3CN—H_2O$ system discerned two minima; a linear complex A and cyclic complex B. Interaction energies computed at B3LYP/6-311++G(d,p) level of theory showed complex A to be more stable than complex B. Experimentally, the formation of the complex A was evidenced from the blue-shift and red-shift in the C≡N and O—H stretching vibrational modes of CH_3CN and H_2O sub-molecules, respectively. The experimental vibrational wavenumbers agreed well with the computed wavenumbers carried out at B3LYP/6-311++G(d,p) level of theory. The Onsager Self-Consistent Reaction Field model showed that complex A is stabilized more in N_2 and Ar matrices, which supports our experimental observation. NBO analysis showed that the hyperconjugative interaction is operative in both complexes A and B.

Acknowledgement

R.G. acknowledges the grant of a research fellowship from, IGCAR, Department of Atomic Energy, India.

Appendix A. Supplementary material

Supplementary data associated with this article can be found, in the online version, at http://dx.doi.org/10.1016/j.molstruc.2015.03.046.

References

[1] http://science.gsfc.nasa.gov/691/cosmicice/interstellar.html.
[2] O.W. Kolling, Anal. Chem. 59 (1987) 674.
[3] T.B. Freedman, E.R. Nixon, Spectrochim. Acta 28A (1972) 1375.
[4] H.S. Kim, K. Kim, Bull. Korean Chem. Soc. 13 (1992) 521.
[5] A. Givan, A. Loewenschuss, J. Mol. Struct. 98 (1983) 231.
[6] S. Coussan, Y. Boutelier, J.P. Perchard, V. Brenner, P. Millié, W.Q. Zheng, F. Talbot, J. Chem. Phys. 110 (1999) 10046.
[7] E. Kryachko, M.T. Nguyen, J. Phys. Chem. A 106 (2002) 4267.
[8] S.C. White, H.W. Thompson, Proc. R. Soc. London A 291 (1966) 460.
[9] M.S. Sousa Lopes, H.W. Thompson, Spectrochim. Acta 24A (1968) 1367.
[10] S.S. Mitra, J. Chem. Phys. 36 (1962) 3286.
[11] A. Allerhand, P.V.R. Schelyer, J. Am. Chem. Soc. 85 (1963) 371.
[12] N.P. Wells, J.A. Phillips, J. Phys. Chem. A 106 (2002) 1518.
[13] R. Hattori, E. Suzuki, K. Shimizu, J. Mol. Struct. 750 (2005) 123.
[14] N. Goldberg, S.R. Lubell, B.S. Ault, J. Mol. Struct. 740 (2005) 125.
[15] A.B. Baker, C. Samet, J.T. Lyon, L. Andrews, J. Phys. Chem. A 109 (2005) 8280.
[16] L. Schriver, A. Schriver, S. Racine, J.P. Perchard, Chem. Phys. 119 (1988) 95.
[17] Y. Gu, T. Kar, S. Scheiner, J. Mol. Struct. 552 (2000) 17.
[18] W.P. Schroeder, K. Chenoweth, C.E. Dykstra, Chem. Phys. Lett. 373 (2003) 8.
[19] E. Sanchez-Garcıa, A. Mardyukov, A. Tekin, R. Crespo-Otero, L.A. Montero, W. Sander, G. Jansen, Chem. Phys. 343 (2008) 168.
[20] E.L. Zins, L. Krim, Phys. Chem. Chem. Phys. 16 (2014) 3388.
[21] R. Gopi, N. Ramanthan, K. Sundararajan, J. Mol. Struct. 1083 (2015) 364.
[22] Doo-Sik Ahn, Sungyul Lee, Bull. Korean Chem. Soc. 24 (2003) 545.
[23] A. Chaudhari, S. Lee, Int. J. Quantum Chem. 102 (2005) 106.
[24] E. Rissi, E.E. Fileti, S. Canuto, Theor. Chem. Acc. 110 (2003) 360.
[25] I. Bako, T. Megyes, G. Palinkas, Chem. Phys. 316 (2005) 235.
[26] T. Takamuku, M. Tabata, A. Yamaguchi, J. Nishimoto, M. Kumamoto, H. Wakita, T. Yamaguchi, J. Phys. Chem. B 102 (1998) 8880.
[27] G.M. Chaban, J. Phys. Chem. A 108 (2004) 4551.
[28] M.P. Bernstein, S.A. Sandford, L.J. Allamandola, APJ 476 (1997) 932.
[29] M.J. Frisch, G.W. Trucks, H.B. Schlegel, P.M.W. Gill, B.G. Johnson, M.A. Robb, J.R. Cheeseman, T. Keith, G.A. Petersson, J.A. Montgomery, K. Raghavachari, M.A. Al-Laham, V.G. Zakrzewski, J.V. Ortiz, J.B. Foresman, J. Cioslowski, B.B. Stefanov, A. Nanayakkara, M. Challacombe, C.Y. Peng, P.Y. Ayala, W. Chen, M.W. Wong, J.L. Andres, E.S. Replogle, R. Gomperts, R.L. Martin, D.J. Fox, J.S. Binkley, D.J. Defrees, J. Baker, J.P. Stewart, M. Head-Gordon, C. Gonzalez, J.A. Pople, GAUSSIAN 94, Revision D.1, Gaussian Inc., Pittsburgh, PA, 1995.
[30] S.F. Boys, F. Bernardi, Mol. Phys. 19 (1970) 553.
[31] R.F.W. Bader, Atoms in Molecules. A Quantum Theory, Clarendon Press, Oxford, 1994.
[32] F. Biegle-Koning, R.F.W. Bader, W.H. Tang, J. Comput. Chem. 96 (2000) 6796 (AIM 2000, Version 1).

[33] R.G.A. Bone, R.F.W. Bader, J. Phys. Chem. 100 (1996) 10892.
[34] E.D. Glendening, J.E. Carpenter, F. Weinhold, NBO version 3.1.
[35] L. Onsager, J. Am. Chem. Soc. 58 (1936) 1486.
[36] M.W. Wong, M.J. Frisch, K.B. Wiberg, J. Am. Chem. Soc. 113 (1991) 4776.
[37] R.M. Bentwood, A.J. Barnes, W.J. Orville-Thomas, J. Mol. Spect. 84 (1980) 391.
[38] L. Schriver, A. Schriver, J.P. Perchard, J. Chem. Soc. Faraday Trans. 81 (1985) 1407.
[39] S. Pilla, J.A. Hamida, K.A. Muttalib, N.S. Sullivan, Phys. Lett. A 256 (1999) 75.
[40] M.E. Jacox, J. Phys. Chem. Ref. Data, Monogr. 3 (1994).
[41] M.J.T. Jordan, J.E. Del Bene, J. Am. Chem. Soc. 122 (2000) 2101.
[42] F. Weinhold, J. Mol. Struct. (Theochem.) 181 (1997) 398.
[43] G.L. Sosa, N.M. Peruchena, R.H. Conteras, E.A. Castro, J. Mol. Struct. (Theochem.) 219 (2002) 577.
[44] P. Kolandaivel, V. Nirmala, J. Mol. Struct. 33 (2004) 694.
[45] Y.X. Lu, J.W. Zou, Y.H. Wang, Y.J. Jiang, Q.S. Yu, J. Phys. Chem. A 111 (2007) 10781.
[46] W. Wang, P. Hobza, J. Phys. Chem. A 112 (2008) 4114.
[47] N.J.M. Amezaga, S.C. Pamies, N.M. Peruchena, G.L. Sosa, J. Phys. Chem. A 114 (2010) 552.
[48] W. Wang, J. Phys. Chem. A 115 (2011) 9294.
[49] M. Jablonski, M. Palusiak, J. Phys. Chem. A 116 (2012) 2322.
[50] M. Solimannejad, M. Malekani, J. Phys. Chem. A 117 (2013) 5551.
[51] W. Zierkiewicz, D. Michalska, Z. Havlas, P. Hobza, Chem. Phys. Chem. 3 (2002) 511.
[52] P. Hobza, Z. Havla, Theor. Chem. Acc. 108 (2002) 325.
[53] W. Zierkiewicz, P. Jurecka, P. Hobza, Chem. Phys. Chem. 6 (2005) 609.
[54] I.V. Alabugin, M. Manoharan, S. Peabody, F. Weinhold, J. Am. Chem. Soc. 125 (2003) 5973.
[55] J. Joseph, E.D. Jemmis, J. Am. Chem. Soc. 129 (2007) 4620.